

See discussions, stats, and author profiles for this publication at: <https://www.researchgate.net/publication/318244897>

Climate warming over the past half century has led to thermal degradation of permafrost on the Qinghai–Tibet Plateau

Article in *The Cryosphere* · February 2018

DOI: 10.5194/tc-12-595-2018

CITATIONS

18

READS

726

3 authors:



Ran Youhua

Chinese Academy of Sciences

51 PUBLICATIONS 1,305 CITATIONS

SEE PROFILE



Xin Li

Chinese Academy of Sciences

304 PUBLICATIONS 6,417 CITATIONS

SEE PROFILE



Guodong Cheng

Chinese Academy of Sciences

343 PUBLICATIONS 9,994 CITATIONS

SEE PROFILE

Some of the authors of this publication are also working on these related projects:



ARC Linkage project [View project](#)



Heihe Remote Sensing Experiment [View project](#)



Climate warming over the past half century has led to thermal degradation of permafrost on the Qinghai–Tibet Plateau

Yuhua Ran^{1,2}, Xin Li^{1,2,3}, and Guodong Cheng^{1,4}

¹Key Laboratory of Remote Sensing of Gansu Province, Heihe Remote Sensing Experimental Research Station, Cold and Arid Regions Environmental and Engineering Research Institute, Chinese Academy of Sciences, Lanzhou 730000, China

²University of Chinese Academy of Sciences, Beijing 100049, China

³CAS Center for Excellence in Tibetan Plateau Earth Sciences, Beijing 100101, China

⁴Institute of Urban Studies, Shanghai Normal University, Shanghai 200234, China

Correspondence: Xin Li (lixin@lzb.ac.cn)

Received: 27 June 2017 – Discussion started: 6 July 2017

Revised: 27 December 2017 – Accepted: 17 January 2018 – Published: 21 February 2018

Abstract. Air temperature increases thermally degrade permafrost, which has widespread impacts on engineering design, resource development, and environmental protection in cold regions. This study evaluates the potential thermal degradation of permafrost over the Qinghai–Tibet Plateau (QTP) from the 1960s to the 2000s using estimated decadal mean annual air temperatures (MAATs) by integrating remote-sensing-based estimates of mean annual land surface temperatures (MASTs), leaf area index (LAI) and fractional snow cover values, and decadal mean MAAT date from 152 weather stations with a geographically weighted regression (GWR). The results reflect a continuous rise of approximately $0.04^{\circ}\text{C a}^{-1}$ in the decadal mean MAAT values over the past half century. A thermal-condition classification matrix is used to convert modelled MAATs to permafrost thermal type. Results show that the climate warming has led to a thermal degradation of permafrost in the past half century. The total area of thermally degraded permafrost is approximately $153.76 \times 10^4 \text{ km}^2$, which corresponds to 88 % of the permafrost area in the 1960s. The thermal condition of 75.2 % of the very cold permafrost, 89.6 % of the cold permafrost, 90.3 % of the cool permafrost, 92.3 % of the warm permafrost, and 32.8 % of the very warm permafrost has been degraded to lower levels of thermal condition. Approximately 49.4 % of the very warm permafrost and 96 % of the likely thawing permafrost has degraded to seasonally frozen ground. The mean elevations of the very cold, cold, cool, warm, very warm, and likely thawing permafrost areas increased by 88, 97, 155, 185, 161, and 250 m, respec-

tively. The degradation mainly occurred from the 1960s to the 1970s and from the 1990s to the 2000s. This degradation may lead to increased risks to infrastructure, reductions in ecosystem resilience, increased flood risks, and positive climate feedback effects. It therefore affects the well-being of millions of people and sustainable development at the Third Pole.

1 Introduction

Permafrost is defined as earth materials, including ice or organic material, that remain at or below 0°C for at least 2 years (Permafrost Subcommittee, National Research Council of Canada, 1988; Williams and Smith, 1989). An increase in air temperatures often thermally degrades permafrost, which has widespread impacts on engineering design, construction, resource development, carbon and water cycles, and ecological protection in cold regions (Collett, 2002; Cheng and Wu, 2007; Tarnocai et al., 2009; Schuur et al., 2009; Schaefer et al., 2011; Hinzman et al., 2013; Mu et al., 2015; Zhu et al., 2016). In terms of middle- and high-elevation permafrost regions, the area of permafrost in the Qinghai–Tibet Plateau (QTP) is the largest in the world. The permafrost in the QTP experiences higher temperatures than those observed in Siberia and the Arctic, which are more sensitive to global climate warming and human activity (Wu et al., 2002; Haeberli and Hohmann, 2008; Li et al., 2008; Ran et al., 2012; Ran and Li, 2016).

regression coefficients associated with m explanatory factors, i.e., the six independent variables selected by a stepwise linear regression analysis (see below). \mathbf{X} is a matrix of explanatory factors ($n \times m$); $\mathbf{W}(\mu_i, v_i)$ is the spatial weight matrix, which is a diagonal matrix; \mathbf{Y} is a vector ($n \times 1$) for the dependent variables, i.e., the decadal mean MAAT in the 1960s, 1970s, 1980s, 1990s, and 2000s; and n is the number of MAAT observation stations for each year.

In this study, the Gaussian function is used as a spatial weighting function, as shown in Eq. (3):

$$\mathbf{W}(\mu_i, v_i) = \exp\left(-\frac{1}{2}\left(\frac{d_i}{r}\right)^2\right), \quad (3)$$

where d_i is the distance between the i th observation station and the point to be estimated, and r is the bandwidth parameter. To accommodate different station densities, the corrected Akaike information criterion (AIC) is used to determine the optimal bandwidth parameters.

A stepwise linear regression analysis is used to select the independent variables for the GWR model. The variance inflation factor (VIF) is used to assess the multicollinearity of the model. The GWR is implemented in System for Automated Geoscientific Analyses (SAGA) (Conrad et al., 2015), using the GWR for multiple predictor grids, as a geoprocessing tool with a Gaussian weighting function, and a global search range.

Due to the unavailability of vegetation, snow cover, and LST datasets during the 1960s to 2000s, the effects of the dynamics of vegetation, snow cover, and LST on estimating MAAT during this period are unknown, and will inevitably cause some errors in the estimation of MAAT. Recent studies of the QTP show overall that vegetation increased during the past 30 years and snow cover decreased during the past 15 years (Wang et al., 2016; Huang et al., 2017). The effect of vegetation and snow cover change on MAAT and related feedback processes are highly complex. For example, the vegetation–snow interaction effect on MAAT is related to humidity (Zhong et al., 2010; T. Wang et al., 2013; Wu et al., 2015; Yuan et al., 2017). However, we believe that such effects mainly occur at the local level in vegetation dominated areas (Wang et al., 2016; Huang et al., 2017), and they can be partially compensated by in situ time-series MAAT measurements over the QTP for the past 50 years.

2.3 Evaluation of the rate of permafrost thermal degradation

A linear regression model is used to evaluate the rates of MAAT change in the QTP over the past 50 years, and the statistical significance of the regression model is evaluated using Student's t test. Thirteen elevation ranges (<3600, 3600–3800, 3800–4000, 4000–4200, 4200–4400, 4400–4600, 4600–4800, 4800–5000, 5000–5200, 5200–5400, 5400–5600, 5600–5800 m, and >5800 m) are used to evaluate the elevation dependence of the warming rate.

The degradation of permafrost thermal condition is assessed from two perspectives, the change in area of the different permafrost types and the spatial heterogeneity of the change. For the area change, we determined the total area of each permafrost type during the past five decades and calculated the rate of change (i.e., the degradation rate) using the linear regression model. The spatial pattern of the degradation of permafrost thermal condition is assessed at two levels. At the pixel level the spatial distribution of the degradation is evaluated, and at the level of the permafrost types a transfer matrix is used to evaluate the conversions among the types (Stehman, 1997). We also analyse the changes in the elevation histograms for each permafrost type over the past 50 years.

2.4 Datasets

2.4.1 Mean annual land surface temperature

MODIS Terra/Aqua daytime and nighttime LST products (MOD11A1 and MYD11A1, version 5) with a spatial resolution of 1 km and covering 2006 to 2010 were acquired from the Distributed Active Archive Center (DAAC) operated by the U.S. National Aeronautics and Space Administration (NASA). These data are used in this study to estimate MASTs. A pragmatic approach proposed by Ran et al. (2015) is employed to estimate the MASTs using the four daily MODIS LST products. This approach assumes that the arithmetic average of the daytime and nighttime LSTs represent the daily mean LST with acceptable accuracy, and that the daily amplitude of LST is more homogeneous than the LST itself (Liu et al., 2006; Kogan et al., 2011; Ran et al., 2015). This approach allows the full use of every value at any time in any pixel of the MODIS LST products through the use of the temporally and spatially complete LST daily amplitude, which is interpolated using a gap-filling algorithm (Garcia, 2010). This algorithm employs a penalized least squares regression based on discrete cosine transforms that explicitly utilize information from a time series to predict the missing values. The penalized least squares regression is a thin-plate spline smoother for a generally one-dimensional data array, and it can trade off fidelity to the data versus the roughness of the mean function (Garcia, 2010; Wang et al., 2012). This approach is easy to implement and independent of other observations. Validation shows that the scheme is effective in restoring the missing values in MODIS instantaneous LST observations and produces a spatially and temporally continuous daily average LST dataset that displays good agreement with observations made at the ground surface. The errors in the results originate mainly from the original instantaneous LST MODIS products. A more detailed description of this scheme can be found in Ran et al. (2015). The temporally and spatially continuous daily mean LSTs from 1 January 2006 to 31 December 2010 and the corresponding MASTs used in this study are produced using the above approach.

2.4.2 Fractional snow cover

Arithmetic mean values of daily cloudless FSC products from 2006 to 2010 are used in this study. This product is derived from the daily MODIS 500 m snow cover product (MOD10A1) using a gap filling process based on a cubic spline interpolation algorithm. A comparison with reference fractional snow cover (FSC) data obtained from Landsat Enhanced Thematic Mapper Plus (ETM+) shows the high accuracy with which this product reflects snow cover information over the QTP (Tang et al., 2013). The cloudless FSC products were acquired from the Cold and Arid Regions Science Data Center, Lanzhou, China (<http://westdc.westgis.ac.cn>).

2.4.3 Leaf area index

Annual mean leaf area index (LAI) values obtained from the Global Land Surface Satellite (GLASS), which make up a high-quality LAI product with an 8-day temporal resolution and a 1 km spatial resolution and cover the period from 2006 to 2010, are used in this study. The GLASS LAI product is derived from the fused MODIS and CYCLOPES LAI products, and the remaining effects of cloud contamination have been removed using MODIS time series surface reflectance data and general regression neural networks (Xiao et al., 2014). The results of validation show that the GLASS LAI product has a lower uncertainty than the MODIS and CYCLOPES LAI products (Xiang et al., 2014). The GLASS LAI product was acquired from the GLASS project website (<http://glass-product.bnu.edu.cn>).

2.4.4 In situ MAAT observations

The MAAT measurements, which were collected at 131 stations for the 1960s and 1970s, 133 stations for the 1980s, 144 stations for the 1990s, and 152 stations for the 2000s within the QTP and the surrounding area, were acquired from the data centre of the China Meteorological Administration (<http://cdc.nmic.cn>). The distribution of the 152 stations for the 2000s is shown in Fig. 1. The density of stations in the eastern QTP is higher than in earlier years. The decadal mean MAAT values over the past five decades are used in this study.

2.4.5 Validation data

Validation of the long-term permafrost thermal condition is difficult due to the limited amounts of reference data that are available. In this study, we evaluate the results by comparing the estimated permafrost distribution in the 2000s with previous regional-scale permafrost maps and borehole measurements at individual sites. The permafrost maps that cover the QTP from Li and Cheng (1996), Nan et al. (2002), and Zou et al. (2017) are used at the regional scale. In particular, the map of Zou et al. (2017) integrates the MODIS 8-day LST product within the framework of the temperature at the top of the

Table 2. The statistics of the stepwise linear regression analysis.

Model	Independent variables	Adjusted R^2
1	MAST	0.83
2	MAST, LAI	0.87
3	MAST, LAI, FSC	0.88
4	MAST, LAI, FSC, elevation	0.90
5	MAST, LAI, FSC, elevation, longitude	0.91
6	MAST, LAI, FSC, elevation, longitude, latitude	0.93

permafrost (TTOP) model (Smith and Riseborough, 1996), and careful validation of this map has been performed using MAGT data. At the site scale, the MAGT values used in this study were collected from 142 boreholes presented in the existing literature (Yu et al., 2008; Q. F. Wang et al., 2013; Luo et al., 2013) and the International Permafrost Association's International Polar Year Thermal State of Permafrost Snapshot Borehole Inventory, downloaded from the National Snow and Ice Data Center (NSIDC) (<http://nsidc.org>) (International Permafrost Association, 2010). The distribution of these boreholes is shown in Fig. 1.

2.4.6 Ancillary data

The distribution of water bodies in the MODIS land cover product (MOD12Q1) and the map showing the distribution of glacier ice from the second Chinese glacier inventory are used to support the permafrost area statistics. The MOD12Q1 product is used for consistency with the other remote sensing products employed in this study. Conversely, the glacier extents from the second Chinese glacier inventory are compiled based on Landsat Thematic Mapper (TM) or ETM+ images acquired from 2004 to 2011, as well as other ancillary data, such as DEMs. The robust band ratio segmentation method is first used to delineate the glacier outlines, and intensive manual improvements are then performed to improve its accuracy. An error assessment shows that the area error for all of the glaciers in China is approximately 3.2 % (Guo et al., 2015).

3 Results

Stepwise linear regression analysis shows that the use of the MAST, the leaf area index (LAI), FSC, elevation, latitude, and longitude as independent variables results in the highest degree of explanatory power for the past five decades, and the significance level is less than 0.0001 (Model 6 in Table 2). The VIF value less than 1.5 shows that the degree of tolerance is high, and the multicollinearity of the model is thus acceptable. The performance of the GWR model in

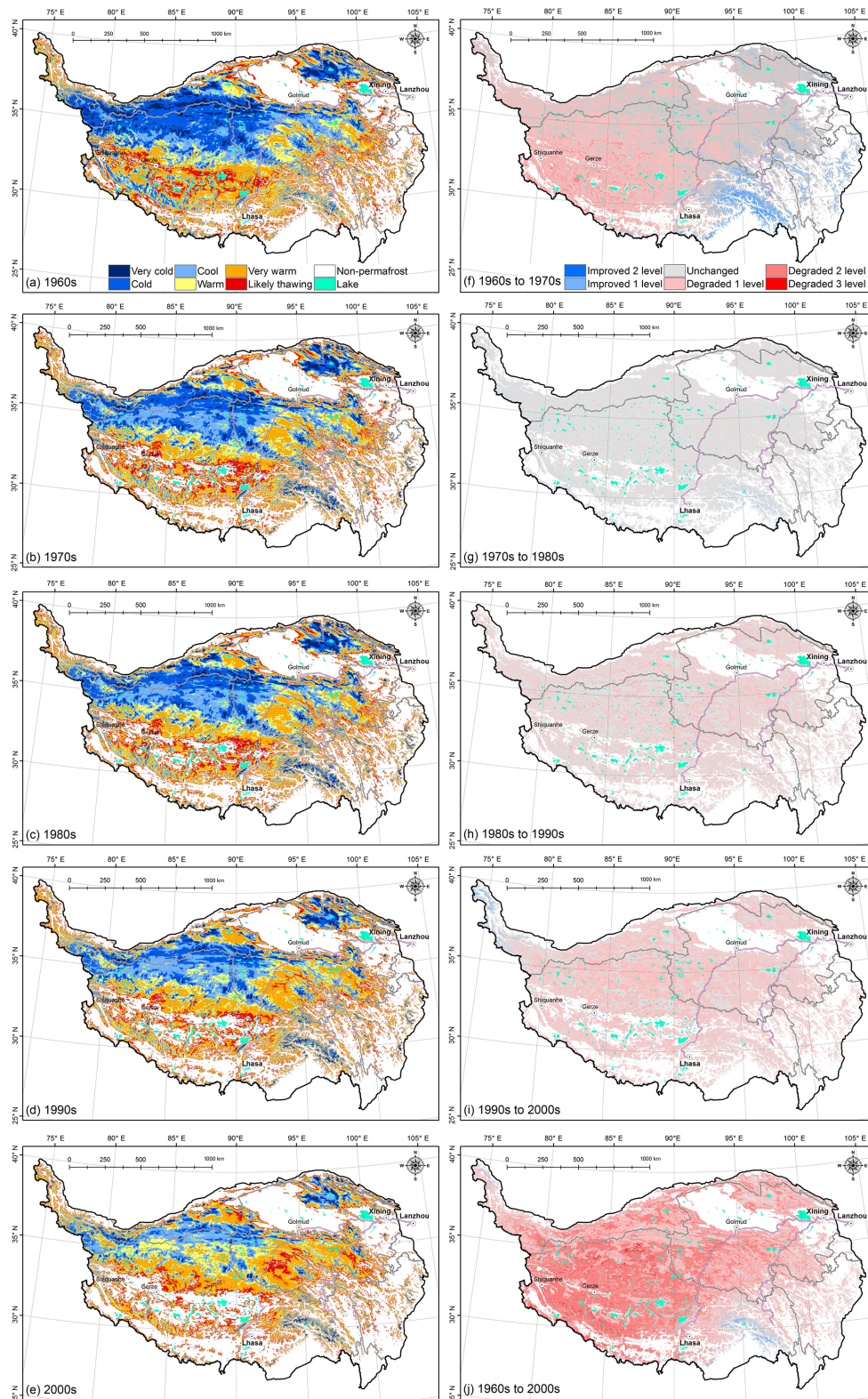


Figure 4. The permafrost map in each decade (a–e) and its spatial changes from the 1960s to the 2000s (f–j) over the QTP during the past 50 years.

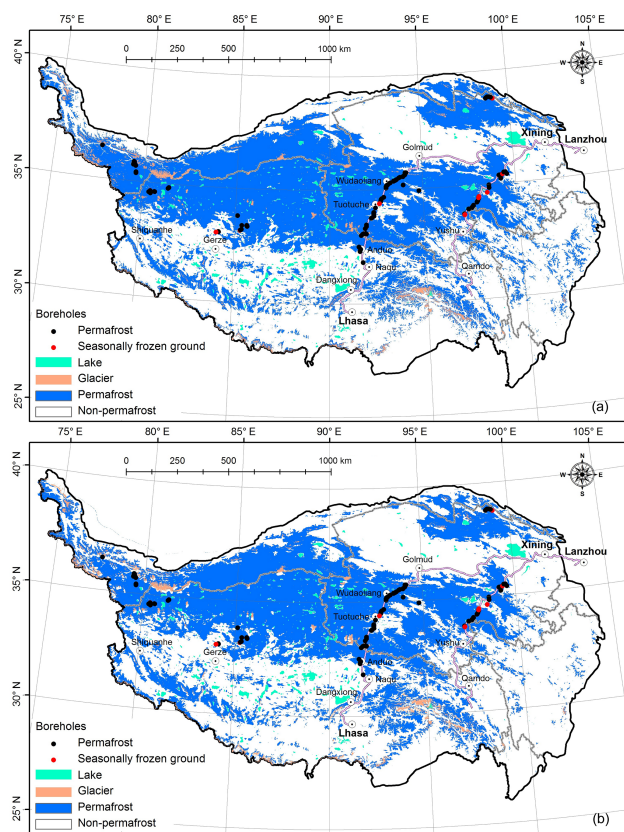


Figure 5. Comparison of the permafrost extent between the results of this study (a) and the permafrost map presented by Zou et al. (2017) (b).

content, groundwater occurrence, geothermal anomalies, and human activity (Stieglitz et al., 2003; Zhang, 2005; Lawrence et al., 2008; Cheng and Jin, 2013; Westermann et al., 2016). For example, the low heat conductivity of soil leads to lag between increases in surface temperatures and the subsequent increase in permafrost temperature or reduction in permafrost thickness (Li et al., 1996). The delay time is longer for permafrost thickness than temperature and varies with the thermal condition (Li et al., 1996; J. Wu et al., 2010). For the cold permafrost, the thermal degradation may be delayed by thermal offset and seasonal offset effects in the permafrost table due to the negative heat budget; i.e., the amount of heat released from the active layer during winter is greater than the amount of heat absorbed in summer (Smith and Riseborough, 2002; J. Wu et al., 2010). For the warm permafrost, a positive heat budget appears in the upper soil layer that leads to a greater spatial degradation rate than that seen in cold permafrost, since the thickness of the warm type is less than that of the cold type (Li et al., 1996; J. Wu et al., 2010). However, the complex physical mechanisms of the interactions between climate change and permafrost are currently poorly understood (Jin et al., 2011), and a large degree of uncertainty may exist in previous evaluations as well as the per-

mafrost area change over the past 50 years in this study. To summarize, despite current warming, large permafrost areas may persist due to the effective thermal inertia of permafrost (Cheng et al., 2012). A final consideration is that the geothermal heat flux leads to thawing of the base of the permafrost (Jin et al., 2006; J. Wu et al., 2010). However, the MAAT model cannot reflect the change of geothermal flux from the crustal interior. Additionally, the geothermal flux data are generally limited or unavailable. The missing geothermal heat flux may lead to a delay in permafrost degradation, especially for the cold permafrost, because the geothermal flux is independent of air temperature. Thirdly, although the resolution of the simulation has been significantly improved to 1 km, it is still coarse relative to the degradation rate of mountain permafrost. The degradation of mountain permafrost is presented in terms of the increase in the elevation of the lower limit of the permafrost, which is generally ~ 100 m. A 1 km change in the horizontal extent change may correspond to a change in elevation of hundreds of metres. Finally, the lack of long-term MAAT measurements in the glacier- and snow-dominated high mountain regions may lead to errors in the estimated MAATs.

Overall, the accelerated degradation effect of the MAAT model may be partly counteracted by the delayed degradation effect of the missing geothermal heat flux component thermal inertia of permafrost. However, long-term observation shows that the mean increasing rate of ground temperature at 10–20 m depth in the QTP is approximately 0.024°C (Zhao et al., 2010; Q. B. Wu et al., 2010; Jin et al., 2011), which is comparable with the warming rate of air temperature. This shows that the evaluation results of permafrost thermal degradation using the MAAT model are generally acceptable at the overall QTP scale.

4.2 The implications of the degradation of thermal condition

The degradation of the permafrost thermal condition in the QTP has important impacts on the safety of infrastructure in permafrost regions, water quality, ecosystem health, and the feedback for regional and global climates. Firstly, as the permafrost thermally degrades, the risk of deterioration and damage to engineered structures in permafrost zones will likely increase. This suggests that the measures used to prevent permafrost degradation may need to be enhanced for new structures. For example, permafrost accounted for 90.1 % of a 10 km long segment of the QTR from Golmud to Lhasa in the 1960s, and these permafrost areas were dominated by the cool type; however, after 50 years (i.e., in the 2000s), these permafrost areas accounted for only 67.77 % and were dominated by the very warm type. For the very warm permafrost, an enhanced measure to prevent permafrost degradation, i.e., the proactive roadbed cooling approach, has been successfully applied in the construction of the QTR (Cheng, 2004, 2005; Cheng et al., 2008). Secondly,

the degradation of permafrost in the QTP may affect the hydrologic cycle in the Third Pole region, which includes the QTP and the surrounding arid regions. Permafrost controls the distribution, recharge, flow paths, discharge, dynamics, and hydrochemistry of groundwater (Cheng and Jin, 2013). The degradation of permafrost affects the interactions among the surface water, subsoil water, and groundwater by changing the hydraulic conductivity and hydraulic connectivity of the soil. The degradation of the ice-rich permafrost itself makes important contributions to surface runoff and the development of thermokarst lakes in the inner Tibetan Plateau (Zhang et al., 2013). The enhanced drainage may lead to increases in flood risk (Larsen et al., 2008) and reductions in ecosystem resilience via seasonal shifts in stream flow and groundwater abundance, because the decrease in permafrost water storage capacity in the QTP will lead to a reduction in dry-season water availability. All of these changes will affect the well-being of millions of people and sustainable development at the Third Pole, which contains the headwater areas of several of the major rivers in Southeast Asia, such as the Yellow, Yangtze, Mekong, Yarlung Zangbo and Shiquan rivers. The Third Pole also includes many inland rivers, such as the Shiyang, Heihe, Shule, and Tarim Rivers in northwestern China. Finally, the permafrost region in the QTP contains approximately 160 Pg of organic carbon (Mu et al., 2015), many thermokarst lakes, and wetlands (Jorgenson et al., 2010; Niu et al., 2011; Luo et al., 2015). Thawing of the permafrost may lead to the drainage or growth of thermokarst lakes (Smith et al., 2005), which may affect greenhouse gas emissions and influence on climate change (Tarnocai et al., 2009; Schuur et al., 2009; Schaefer et al., 2011; McCalley et al., 2014). Additionally, changes in thermokarst lakes may both accelerate and delay permafrost thawing (Westermann et al., 2016; You et al., 2017).

5 Conclusions

This study evaluates likely permafrost thermal degradation over the QTP from the 1960s to the 2000s based on the improved decadal means of the MAATs data over the QTP in the past 50 years obtained by integrating remote-sensing-based MASTs, LAI, and fractional snow cover values, as well as decadal mean MAATs measured at 152 weather stations using a GWR model. Cross validation shows that the accuracy of the estimated permafrost extent is greater than that of previous maps.

The decadal mean MAATs reflect a continuous rise at a rate of approximately $0.04^{\circ}\text{C a}^{-1}$ during the past half century. The warming rate increases with increasing elevation from approximately 0.33°C per decade at 3600 m to 0.49°C per decade at 5200 m and then decreases as elevation increases further. Climate warming has led to the thermal degradation of permafrost in the past half century. The area occupied by the cold permafrost types has continuously de-

creased, and the area occupied by the very warm types has continuously increased. The total degraded area is approximately $153.76 \times 10^4 \text{ km}^2$, which accounts for 87.98 % of the permafrost area in the 1960s. The thermal condition for all permafrost types has degraded to lower levels. The extent of the very cold, cold, and cool types retreated from the south to the north, whereas the extent of the warm, very warm, and likely thawing types extended northward. The mean elevations of the very cold, cold, cool, warm, very warm, and likely thawing types increased by 88, 97, 155, 185, 161, and 250 m, respectively. The degradation mainly occurred during the 1960s to the 1970s and the 1990s to the 2000s. The thermal degradation of permafrost in the QTP has important impacts on the safety of infrastructure, flood risks, ecosystem resilience, and climate feedback, as well as the well-being of millions of people and sustainable development at the Third Pole.

The uncertainties inherent in this analysis cannot be discounted. These uncertainties are due to asynchronous changes in near-surface air temperatures and deep soil layer temperatures, the missing geothermal flux, insufficient resolution, or the inaccuracies and sparseness of the surface station data employed. In order to reduce these uncertainties, a deep layer soil map, surficial geology, and ground ice map are required. All of this will benefit from the accumulation of field data in the future, especially from boreholes.

Data availability. The data used in this paper are available upon request from the corresponding author.

Competing interests. The authors declare that they have no conflict of interest.

Acknowledgements. This study was jointly supported by the Strategic Priority Research Program of the Chinese Academy of Sciences (Grant No. XDA19070204), National Natural Science Foundation of China projects (Grant No. 41471359), and the Youth Innovation Promotion Association of the Chinese Academy of Sciences (Grant No. 2016375). The authors thank the associate editor and three anonymous reviewers for their insightful comments and suggestions that helped improve this paper.

Edited by: Peter Morse

Reviewed by: three anonymous referees

References

- Brown, R. D. and Mote, P. W.: The response of Northern Hemisphere snow cover to a changing climate, *J. Climate*, 22, 2124–2145, 2009.
- Brunsdon, C., Fotheringham, S., and Charlton, M.: Geographically weighted regression, *J. Roy. Stat. Soc. D*, 47, 431–443, 1998.

